Clairvoyant Clutter Mitigation in a Symbol-Based OFDM Radar Receiver

Steven Mercier*, Stéphanie Bidon*, Damien Roque* and Cyrille Enderli†
*ISAE-SUPAERO, Université de Toulouse, France
Email: {steven.mercier,stephanie.bidon,damien.roque}@isae-supaero.fr
†Thales DMS, Élancourt, France
Email: cyrille-jean.enderli@fr.thalesgroup.com

***Abstract*—This paper investigates clutter rejection techniques in an OFDM symbol-based radar receiver. Two rejection filters that assume known the clutter covariance matrix are proposed. These aim at mitigating not only the clutter main peak but also its noise-like pedestal that leads to target masking issues. Performance is assessed with synthetic data on filters outputs and in terms of signal-to-clutter-plus-noise-ratio. Results show that the proposed methods succeed, to some extent, in uncovering exo-clutter targets. Rejecting clutter within the symbol-based architecture (instead of prior to) is advantageous for slowly-moving targets.**

I. Introduction

The well-known spectrum congestion problem leads to develop innovative solutions to make spectrally coexist different users, especially, radar and communications [1]. Within this framework, a possible solution is to use a unique waveform that *simultaneously* senses the environment and transmits information. To that end, multicarrier waveforms have been considered. Particularly, the so-called OFDM (Orthogonal Frequency-Division Multiplexing) modulation, may be a good candidate [2].

If multicarrier receivers are nowadays well described for communication purposes [3], designing such receivers to detect/estimate targets is an on going process. Indeed, important challenges include dealing with transmitted symbols and reusing receiver's building blocks.

In the literature, two processing architectures can be mainly found [2]: 1) a conventional correlation approach in the time-domain; 2) a symbol-based receiver that enables a low computational complexity while exploiting the multicarrier waveform structure. In both cases, the target response in the range-Doppler domain is characterized by a peak and a noise-like floor [4], [5]. In practice, this pedestal (due to a self-interference phenomenon) is detrimental to detection.

To reveal weak targets hidden in the self-interference-plus-noise floor, CLEAN-inspired techniques have been used to successively remove targets in passive bistatic radar (PBR) [6] and in monostatic radar [7]. However in presence of diffuse component like clutter, more robust techniques have to be considered to remove the latter (including its induced pedestal).

This work has been supported by DGA/MRIS under grant 2017.60.0005 and Thales DMS.

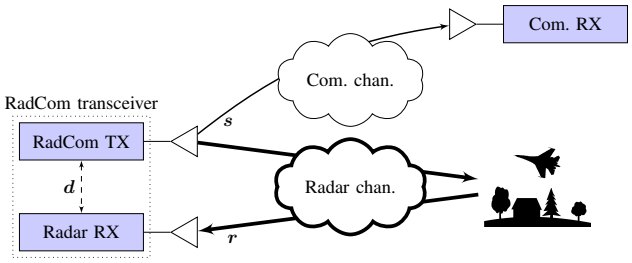

Fig. 1. Illustration of the RadCom channel in presence of clutter. Transmitted symbols of information are known by the radar receiver.

In terrestrial PBR, to filter-out clutter, it is common to use an orthogonal projection to a presumed clutter subspace prior to correlation in the time domain. A series of algorithms known as ECA (Extensive Cancellation Algorithm) have thus been described. The projection may be implemented in the time domain [6], [8], [9] or in the subband domain in case of OFDM waveforms [10]–[13]. However in such scenarios, clutter often reduces to highly coherent components at zero velocity and short ranges. In alternate scenarios with more spread clutter (*e.g.*, in airborne PBR or in monostatic cases), ECA approach may thus lack adaptivity.

In this paper, we focus on the symbol-based architecture in monostatic radar and investigate the performance of *adaptive* clutter canceling (cf. illustration of the so-called RadCom scenario considered in Fig. 1). Particularly, we develop an expression of the clutter covariance matrix prior to processing (including no range compression) and further use it to filter-out clutter at two different stages of the processing.

The remainder of the paper is organized as follows. In Section II we recall the expressions of the symbol-based OFDM radar system studied so far in clutter-free scenarios [5]. In Section III a statistical clutter model is proposed and added to the radar channel. Section IV proposes clairvoyant clutter mitigation filters. Their performance is discussed in terms of signal-to-clutter-plus-noise ratio (SCNR) in Section V. Finally, conclusions and future work are given in Section VI.

In what follows, $\mathcal{I}_N$ stands for the finite set of integers $\{0,\dots,N-1\}$ and $\delta_{.,.}$ for the Kronecker symbol. $\boldsymbol{x} \sim \mathcal{CN}(\boldsymbol{0},\boldsymbol{C})$ refers to a zero-mean circularly symmetric complex Gaussian vector with covariance matrix $\boldsymbol{C}$.

978-1-7281-2660-9/19/$31.00

II. A MODEL OF LOW-COMPLEXITY WCP-OFDM RADAR

The RadCom transmitter sends a multicarrier waveform along K subcarriers over M blocks. Each data symbol $d_{k,m}$ taken in a complex constellation (*e.g.*, phase-shift keying – PSK) is linearly maped to a pulse-shape $g_{k,m}(t) = g(t - mT_0)\exp(j2\pi kF_0 t)$, $(k,m) \in \mathcal{I}_K \times \mathcal{I}_M$, with F_0 the elementary spacing between subcarriers and T_0 the pulse repetition interval. To obtain a low-complexity time-domain implementation of the pulse-shaping operation, we restrict the time support of g to $[0, T_0)$. Such a transmission scheme is referred to as weighted cyclic prefix (WCP)-OFDM [14] and can be seen as a generalization of the traditional CP-OFDM to non-rectangular pulse-shapes. Since the transmitted signal occupies a bandwidth $B \approx KF_0$, its critically sampled expression is given by [5]

$$\boldsymbol{s} = \left[\boldsymbol{I}_M \otimes (\boldsymbol{D_g P F}_K^H)\right] \boldsymbol{d} \tag{1}$$

with $\boldsymbol{d}$ the data symbols vector defined as $[\boldsymbol{d}]_{k+mK} \triangleq d_{k,m}$, $\boldsymbol{F}_K$ the unitary K-DFT matrix, $\boldsymbol{P}$ the $L \times K$ cyclic extension matrix with $L \triangleq T_0 B \geq K$, namely $[\boldsymbol{P}]_{l,k} = \delta_{l,k} + \delta_{l,k+K}$, $\boldsymbol{D_g} = \mathrm{diag}(\boldsymbol{g})$ where $\boldsymbol{g} = [g[0], \ldots, g[L-1]]^T$ is the transmit pulse-shape vector, and $\boldsymbol{I}_M$ the identity matrix of size M.

Let N_t be the number of targets in the illuminated radar scene. These are modeled as single-point scatterers with the following assumptions:

- a constant complex amplitude α_{n_t} during the transmission of $\boldsymbol{s}$ (*i.e.*, coherent processing interval);
- an unambiguous range $R_{0,n_t} \triangleq l_{0,n_t}\Delta_R$ with $l_{0,n_t} \in \mathcal{I}_L$ the range gate and $\Delta_R = c/(2B)$ the range resolution, c being the speed of light;
- a radial velocity v_{n_t} inducing a simple frequency shift of (1) by $F_{d,n_t} = 2v_{n_t}F_c/c \ll B$ with F_c the transceiver's carrier frequency.

The corresponding baseband signal received by the RadCom transceiver and critically sampled at rate B is [5]

$$\boldsymbol{r}_t = \sum_{n_t=0}^{N_t-1} \alpha_{n_t} \boldsymbol{Z}_{n_t} \boldsymbol{s} \tag{2}$$

where $[\boldsymbol{Z}_{n_t}]_{(l,l') \in \mathcal{I}_{LM} \times \mathcal{I}_{LM}} = e^{j2\pi f_{d,n_t} l/L} \delta_{l,l'+l_{0,n_t}}$ is the range-Doppler shift matrix related to the n_tth target, involving its normalized Doppler frequency $f_{d,n_t} = F_{d,n_t} T_0$. Finally, in a clutter-free scenario, the signal observed by the receiver is $\boldsymbol{r} = \boldsymbol{r}_t + \boldsymbol{n}$ with $\boldsymbol{n} \sim \mathcal{CN}(\boldsymbol{0}, \sigma^2 \boldsymbol{I}_{LM})$ the thermal noise.

A 3-stage symbol-based processing inspired from [2] is then performed on the received signal to provide an estimate of the radar scene in the range-Doppler domain, *i.e.*, (i) linear symbol estimation by a (bi)-orthogonal WCP-OFDM receiver; (ii) symbols removal (as they are perfectly known by the receiver); (iii) range-Doppler map computation. It is summed up by [5]:

$$\boldsymbol{x} = \underbrace{(\boldsymbol{F}_M \otimes \boldsymbol{F}_K^H)}_{\text{(iii)}} \underbrace{\boldsymbol{D}_{\boldsymbol{d}}^{-1}}_{\text{(ii)}} \underbrace{[\boldsymbol{I}_M \otimes (\boldsymbol{F}_K \boldsymbol{P}^T \boldsymbol{D}_{\check{\boldsymbol{g}}}^H)]}_{\text{(i)}} \boldsymbol{r} \tag{3}$$

with $\boldsymbol{D}_{\check{\boldsymbol{g}}} = \mathrm{diag}(\check{\boldsymbol{g}})$ where $\check{\boldsymbol{g}} = [\check{g}[0], \ldots, \check{g}[L-1]]^T$ is the receive pulse-shape vector and $\boldsymbol{D}_{\boldsymbol{d}}^{-1} = \mathrm{diag}^{-1}(\boldsymbol{d})$. A typical output obtained for a single-target scenario is displayed in Fig. 3a (see Section V for simulation details).

This low-complexity processing was already shown to create self-interference, resulting in an increased white noise floor in the range-Doppler map and, consequently, in target masking issues [5]. Given that the phenomenon becomes significant with the number of scatterers, their amplitude and their range and/or Doppler, we expect clutter to be highly deleterious for target detection, even in exo-clutter.

III. IMPACT OF GROUND CLUTTER

In this Section, we extend the propagation channel model (2) to account for ground clutter and observe its impact on the symbol-based radar processing (3).

A. Clutter model

Ground clutter is a major interference source in radar. In the range dimension, it can be described as a continuum of scattering elements. In monostatic topologies, clutter is typically present at all ranges up to the radar horizon. Hereafter, the latter is assumed to coincide with the unambigous range.

Let us divide the range dimension into $N_c = pL$ patches ($p \in \mathbf{N}^*$) of resolution $\Delta_c = \Delta_R/p$. Providing that the transmitted WCP-OFDM signal varies slowly on duration $1/(pB)$ and that the radar has an ideal antenna pattern, each clutter patch can be characterized by:

- a complex amplitude γ_{n_c}, which may vary with time;
- a medium range $R_{0,n_c} = l_{0,n_c}\Delta_c$ with $l_{0,n_c} \in \mathcal{I}_{pL}$;
- a constant radial velocity v_{n_c} with corresponding Doppler frequency F_{d,n_c}. As for targets, we assume $F_{d,n_c} \ll B$.

The received clutter signal critically sampled at rate B can thus be expressed at baseband as[1]

$$\boldsymbol{r}_c = \sum_{n_c=0}^{N_c-1} \boldsymbol{\gamma}_{n_c} \odot (\boldsymbol{Z}_{n_c} \boldsymbol{s}) \tag{4}$$

with $\boldsymbol{Z}_{n_c}$ the range-Doppler shift matrix introduced in (2), and $\boldsymbol{\gamma}_{n_c} = [\gamma_{n_c}[0], \ldots, \gamma_{n_c}[LM-1]]^T$. Especially, in the remaining of the paper, it is assumed that for $n_c, n_c' \in \mathcal{I}_{N_c}$,

- $\boldsymbol{\gamma}_{n_c}$ is a zero-mean wide sense stationary sequence, with covariance matrix $\boldsymbol{R}_{\boldsymbol{\gamma}_{n_c}} \triangleq \mathbb{E}\left\{\boldsymbol{\gamma}_{n_c} \boldsymbol{\gamma}_{n_c}^H\right\}$ and power $P_{\gamma_{n_c}}$;
- $\boldsymbol{\gamma}_{n_c}$ and $\boldsymbol{\gamma}_{n_c'}$ are independent, leading to $\mathbb{E}\left\{\boldsymbol{\gamma}_{n_c} \boldsymbol{\gamma}_{n_c'}^H\right\} = \boldsymbol{R}_{\boldsymbol{\gamma}_{n_c}} \delta_{n_c,n_c'}$.

The total signal observed by the radar receiver is finally

$$\boldsymbol{r} = \boldsymbol{r}_t + \boldsymbol{u} \quad \text{with} \quad \boldsymbol{u} = \boldsymbol{r}_c + \boldsymbol{n} \tag{5}$$

the clutter-plus-noise contribution.

We depict in Fig. 3b the range-Doppler map resulting from the addition of some zero-Doppler clutter into the scenario of Fig. 3a (see Section V for simulation details). We observe that the target is then no more visible despite its high-Doppler frequency. This is due to the self-interference induced by clutter. Since the latter behaves as a white noise in the range-Doppler

[1] Eq. (4) is given for $p = 1$ for the sake of conciseness but can easily be extended to $p > 1$.

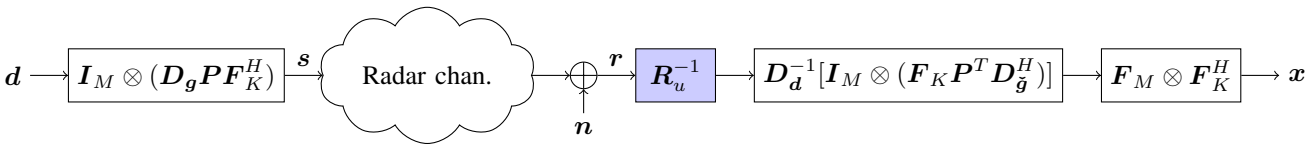

(a) Symbol-based radar receiver with clutter rejection on receive

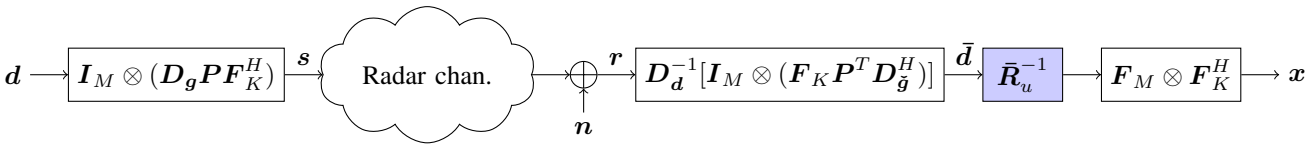

(b) Symbol-based radar receiver with clutter rejection after symbols removal

Fig. 2. Flowchart of two discrete-time WCP-OFDM symbol-based radar systems. Clutter removal is emphasized in colored boxes.

map [5], a conventional clutter filter that rejects only zero-Doppler components fails at removing it. This is exemplified in Fig. 4 where an orthogonal projection has been implemented after stage (ii) of the symbol-based processing (3) as proposed in [12], [13].

B. Clutter-plus-noise covariance matrix

In this work, we investigate the possibility of removing clutter (including its pedestal) in the symbol-based architecture via rejection filters based on the clutter-plus-noise covariance matrix. We especially focus on its expression when conditioned to the data-symbols $\boldsymbol{d}$ which are perfectly known by the radar receiver given the monostatic topology (Fig. 1).

Since clutter and thermal noise are assumed to be independent and zero-mean and using (4), the clutter-plus-noise covariance matrix on receive boils down to

$$\boldsymbol{R}_u \triangleq \mathbb{E}\left\{\boldsymbol{u}\boldsymbol{u}^H|\boldsymbol{d}\right\} = \boldsymbol{R}_c + \sigma^2 \boldsymbol{I}_{LM} \tag{6}$$

with

$$\boldsymbol{R}_c \triangleq \mathbb{E}\left\{\boldsymbol{r}_c \boldsymbol{r}_c^H|\boldsymbol{d}\right\} = \sum_{n_c=0}^{N_c-1} \boldsymbol{R}_{\gamma_{n_c}} \odot \boldsymbol{Z}_{n_c} \boldsymbol{s}\boldsymbol{s}^H \boldsymbol{Z}_{n_c}^H. \tag{7}$$

As justified in the next Section, we also formulate the latter after the second stage of the symbol-based processing (3), *viz*,

$$\bar{\boldsymbol{R}}_u \triangleq \mathbb{E}\left\{\bar{\boldsymbol{d}}_u \bar{\boldsymbol{d}}_u^H|\boldsymbol{d}\right\} = \boldsymbol{T}\boldsymbol{R}_u\boldsymbol{T}^H \tag{8}$$

with $\bar{\boldsymbol{d}}_u \triangleq \boldsymbol{T}\boldsymbol{u}$ the clutter-plus-noise signal after symbols removal and $\boldsymbol{T} \triangleq \boldsymbol{D}_{\boldsymbol{d}}^{-1}[\boldsymbol{I}_M \otimes (\boldsymbol{F}_K \boldsymbol{P}^T \boldsymbol{D}_{\check{\boldsymbol{g}}}^H)]$.

Note that both covariance matrices (6) and (8) entail at the same time the physical clutter components usually located around zero-Doppler as well as its induced pedestal.

IV. Clairvoyant clutter mitigation

In this Section, while we assume matrices (6) and (8) to be known we extend the symbol-based approach of [2] to mitigate clutter.

A. Symbol-based architecture as a mismatched filter

The symbol-based architecture (3) has been originally proposed to exploit the multicarrier structure of the OFDM signal while decreasing the computational complexity compared to matched filtering [2]. Its design ignores the self-interference phenomenon and also removes the known symbols of information [15]. Nonetheless, its goal remains to estimate a radar scene in the range-velocity domain by coherently integrating the received signal according to different range-velocity hypotheses. As such, the symbol-based approach can be seen as a mismatched filter with steering vector

$$\tilde{\boldsymbol{a}}(l,f) = \boldsymbol{T}^H \boldsymbol{f}(l,f) \quad \text{where} \quad \boldsymbol{f}(l,f) = \boldsymbol{e}_d(f) \otimes \boldsymbol{e}_r(l) \tag{9}$$

with

l, f	the tested range-gate and Doppler frequency;
$\boldsymbol{f}(l,f)$	the $(fMK+l)$th column of $\boldsymbol{F}_M^H \otimes \boldsymbol{F}_K$;
$\boldsymbol{e}_d(f)$	the Fourier vector $[\boldsymbol{e}_d(f)]_{m\in\mathcal{I}_M} = e^{j2\pi fm}$;
$\boldsymbol{e}_r(l)$	the Fourier vector $[\boldsymbol{e}_r(l)]_{k\in\mathcal{I}_K} = e^{-j2\pi lk/K}$.

In the following, we propose to evaluate two clutter filters obtained by replacing the steering vector used for matched filtering, denoted $\boldsymbol{a}(l,f)$, by its counterpart (9) in the symbol-based architecture.

B. Clutter rejection on receive

In a single-target scenario, the full received radar signal (5) can be rewritten

$$\boldsymbol{r} = \alpha \boldsymbol{a}(l_0, f_d) + \boldsymbol{u} \tag{10}$$

with $\boldsymbol{a}(l_0, f_d) = \boldsymbol{Z}\boldsymbol{s}$ the target steering vector. In such a problem, the optimal linear filter is well known to be $\boldsymbol{\omega}_{\text{opt}} \propto \boldsymbol{R}_u^{-1}\boldsymbol{a}(l_0, f_d)$ [16]. Accordingly, we propose a first filter as

$$\tilde{\boldsymbol{\omega}}_a \propto \boldsymbol{R}_u^{-1}\tilde{\boldsymbol{a}}(l_0, f_d). \tag{11}$$

Practically, it is tantamount to pre-multiplying the received signal $\boldsymbol{r}$ by the inverse matrix $\boldsymbol{R}_u^{-1}$ and then applying the 3 stages of the symbol-based architecture as depicted in Fig. 2a.

C. Clutter rejection after symbol removal

To fully benefit from the symbol-based structure, we also consider filtering clutter after the second stage of the architecture, namely after symbol removal, on signal

$$\bar{\boldsymbol{d}} \triangleq \boldsymbol{T}\boldsymbol{r} = \alpha \boldsymbol{T}\boldsymbol{a}(l_0, f_d) + \bar{\boldsymbol{d}}_u.$$

Using the same reasoning as in Section IV-B, the second filter is thus

$$\tilde{\boldsymbol{\omega}}_b \propto \bar{\boldsymbol{R}}_u^{-1}\boldsymbol{T}\tilde{\boldsymbol{a}}(l_0, f_d) \propto \bar{\boldsymbol{R}}_u^{-1}\boldsymbol{D}_{\boldsymbol{d}}^{-1}(\boldsymbol{D}_{\boldsymbol{d}}^{-1})^H \boldsymbol{f}(l_0, f_d)$$

which, as we restrict to PSK modulations in the following, reduces to

$$\tilde{\boldsymbol{\omega}}_b \propto \bar{\boldsymbol{R}}_u^{-1}\boldsymbol{f}(l_0, f_d). \tag{12}$$

This filtering approach is illustrated in Fig. 2b. Interestingly, since one has $\boldsymbol{T}\boldsymbol{a}(l_0, f_d) \propto \boldsymbol{f}(l_0, f_d)$ when neglecting the target self-interference [5], filter (12) is optimal up to the presence of the latter.

V. Simulations

Herein, performance of the proposed *clairvoyant* filters (11) and (12) is evaluated in a single-target scenario.

A. Scenario

Data are generated according to (1)-(5) with the following clutter features:

- there is one clutter patch per range gate (*i.e.*, $N_c = L$);
- it is static, namely $f_{d,n_c} = 0$;
- patch's amplitudes follow a circularly-symmetric complex normal distribution, *i.e.*, $\boldsymbol{\gamma}_{n_c} \sim \mathcal{CN}(\boldsymbol{0}, \boldsymbol{R}_{\gamma_{n_c}})$;
- they have the same covariance matrix $\boldsymbol{R}_{\gamma_{n_c}} = \boldsymbol{R}_\gamma$ and power $P_{\gamma_{n_c}} = P_\gamma$;
- they have a Gaussian Doppler spectrum [17], hence for $(l, m), (l', m') \in \mathcal{I}_L \times \mathcal{I}_M$,

$$[\boldsymbol{R}_\gamma]_{l+mK, l'+m'K} = P_\gamma e^{-\varsigma_v^2 |m-m'|^2}$$

with ς the normalized velocity standard deviation.

Parameters values used for simulations are provided in Table I. Particularly, P_γ is chosen to ensure a given theoretical post-processing clutter-to-noise-ratio defined as [5]

$$\text{CNR}_{\text{th}} = \frac{P_\gamma MK}{\sigma^2 \sigma_{d^{-1}}^2 \left\|\check{\boldsymbol{g}}\right\|^2 / K} \tag{13}$$

with $\sigma_{d^{-1}}^2 \triangleq \mathbb{E}\left\{1/|d_{k,m}|^2\right\}$ and $\|\cdot\|$ the ℓ_2 norm. The latter actually corresponds to a scenario where all clutter patches would be located at zero range and Doppler; though unrealistic this scenario is self-interference-free.

B. Results

1) Single runs: We represent in Fig. 5 the range-Doppler maps resulting from the proposed clutter rejection strategies. Compared to that of Fig. 3b, both clutter main component (at zero-Doppler) and its self-interference have been mitigated, thereby uncovering the target from the noise-like background. Particularly at zero-Doppler and beyond range bin 30, we observe that clutter is better rejected after symbol-removal, *i.e.*, by filter $\tilde{\boldsymbol{\omega}}_b$.

TABLE I
Simulation parameters

Parameter	Variable	Value
Number of subcarriers	K	128
Number of blocks	M	32
Expansion factor	L/K	12/8
Constellation	$\boldsymbol{d}$	QPSK
Pulse-shapes	$(\boldsymbol{g}, \check{\boldsymbol{g}})$	TFL [18]
Input noise power	σ^2	0 dB
Theoretical output SNR	SNR_{th}	22 dB
Theoretical output CNR	CNR_{th}	20 dB
Normalized velocity standard deviation	ς_v	0.125

2) SCNR: Herein we quantify the performance of the proposed clutter rejection filters in terms of signal-to-clutter-plus-noise-ratios (SCNR) which is usually a good indicator of detection performance. The SCNR obtained at the output of filters (11) and (12) are given for a unitary power target by, respectively,

$$\text{SCNR}(\tilde{\boldsymbol{\omega}}_a) = \frac{|\tilde{\boldsymbol{\omega}}_a^H \boldsymbol{a}(l_0, f_d)|^2}{\tilde{\boldsymbol{\omega}}_a^H \boldsymbol{R}_u \tilde{\boldsymbol{\omega}}_a} \tag{14}$$

and

$$\text{SCNR}(\tilde{\boldsymbol{\omega}}_b) = \frac{|\tilde{\boldsymbol{\omega}}_b^H \boldsymbol{T}\boldsymbol{a}(l_0, f_d)|^2}{\tilde{\boldsymbol{\omega}}_b^H \bar{\boldsymbol{R}}_u \tilde{\boldsymbol{\omega}}_b}. \tag{15}$$

Both are displayed in Figs. 6-7. Outside the clutter notch located around zero Doppler, the SCNRs values decrease with the target range l_0 and/or Doppler f_d. In fact, as the latter rises, the self-interference induced by the target, which is basically ignored by the filters, gets enhanced [5]. In that region, the filter after symbol-removal $\tilde{\boldsymbol{\omega}}_b$ incurs a slight deterioration compared to that on receive $\tilde{\boldsymbol{\omega}}_a$. The former seems however substantially favorable for slowly moving targets.

VI. Conclusions and future work

In this paper, clutter mitigation is investigated in an existing symbol-based OFDM radar receiver. We implement two clairvoyant rejection filters (*i.e.*, known clutter covariance matrix) to remove its main component along with its noise-like pedestal responsible for target masking. They are proposed at two different stages of the processing (on receive and after data-symbol removal). Their performance is assessed in a single-target scenario in terms of signal-to-clutter-plus-noise-ratio. Results suggest that the filter applied after symbol removal is better suited for detecting slow targets. In any event, in real-world applications, the clutter covariance matrix needs to be estimated.

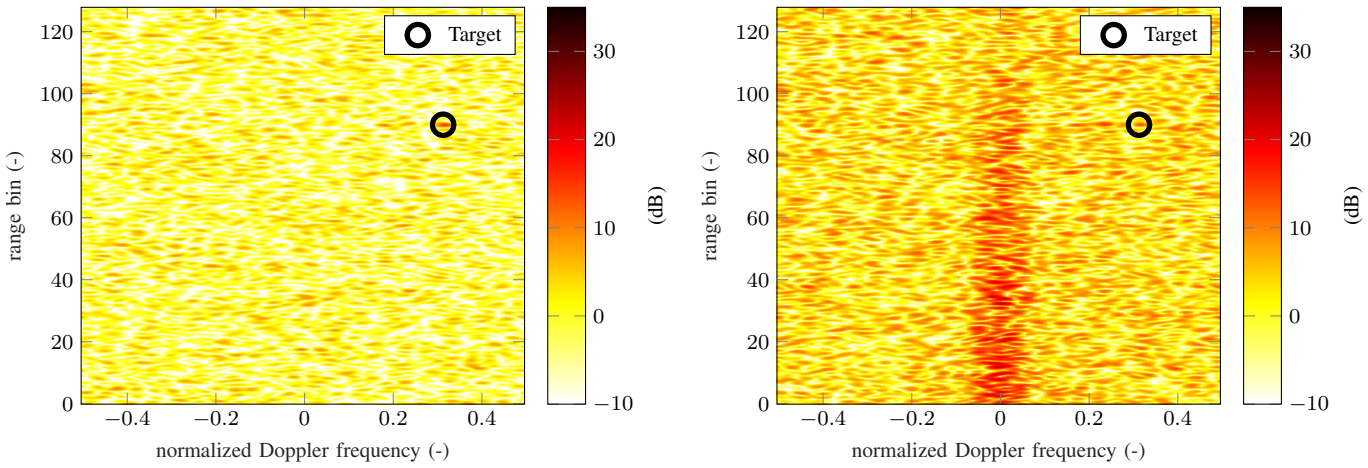

(a) Without clutter

(b) Including clutter

Fig. 3. Typical range-Doppler maps obtained with the symbol-based radar receiver. The clutter self-interference is responsible for masking the target.

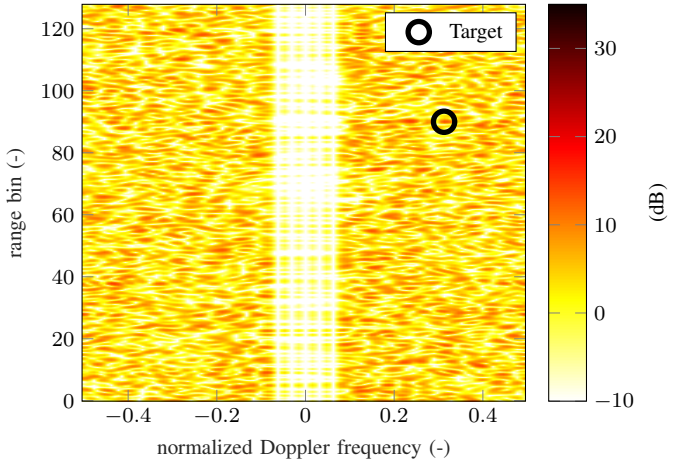

Fig. 4. Range-Doppler map obtained with the symbol-based radar receiver after orthogonal projection following step (ii) and ignoring self-interference [12], [13]. The clutter self-interference remains intact and still masks the target.

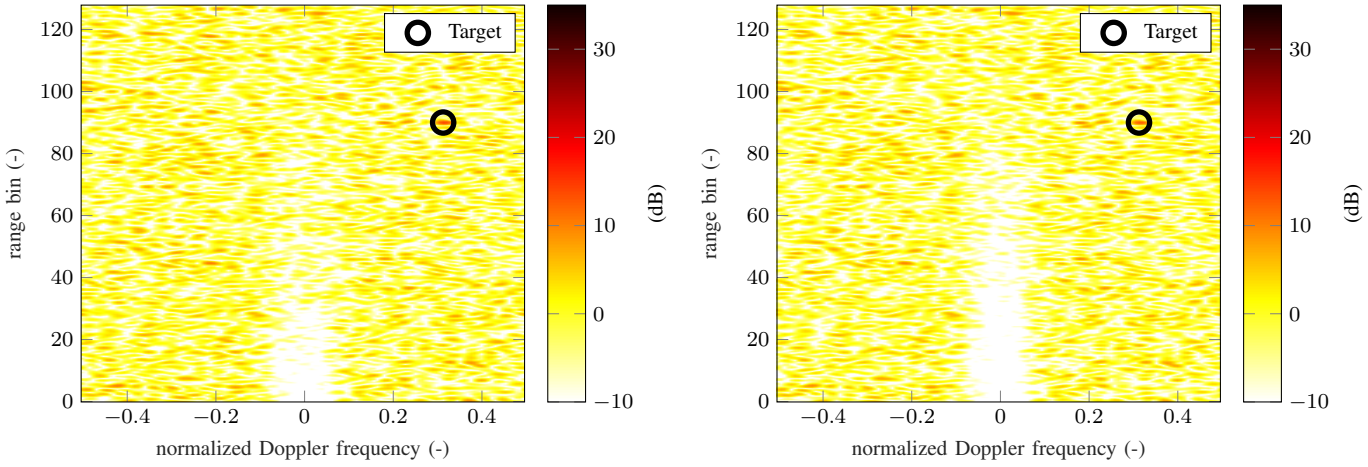

(a) Clutter rejection on receive

(b) Clutter mitigation after symbol removal

Fig. 5. Range-Doppler maps obtained after clairvoyant symbol-based clutter mitigation. Clutter including its pedestal is partially removed so that the target stands out against the background.

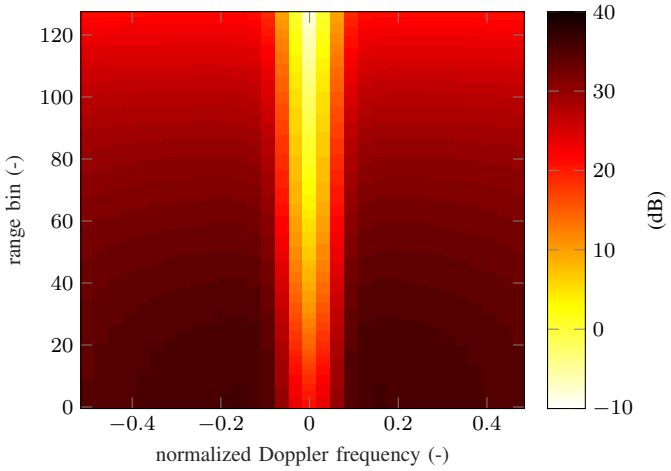

(a) Clutter mitigation on receive

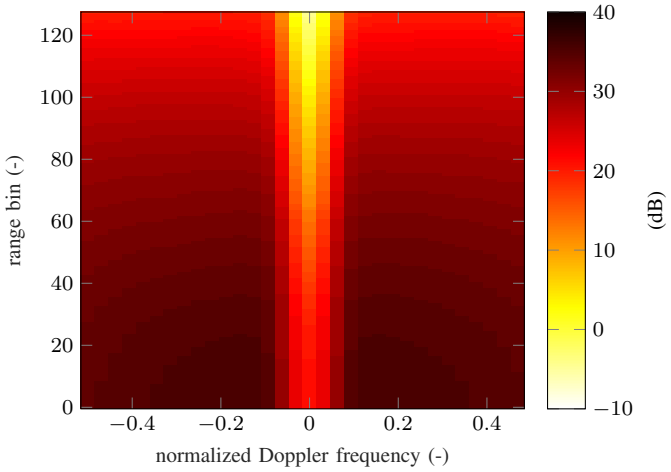

(b) Clutter mitigation after symbol removal

Fig. 6. SCNRs following clairvoyant clutter rejection.

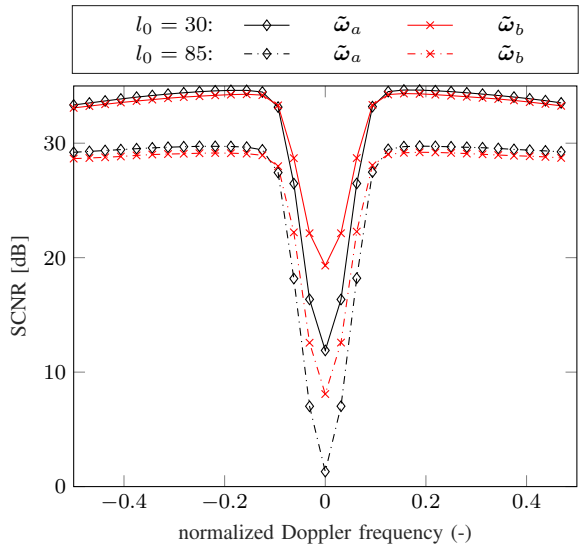

Fig. 7. SCNRs cuts at two different range values.

REFERENCES

[1] B. Paul, A. R. Chiriyath, and D. W. Bliss, "Survey of RF communications and sensing convergence research," *IEEE Access*, vol. 5, pp. 252–270, 2017.

[2] C. Sturm and W. Wiesbeck, "Waveform design and signal processing aspects for fusion of wireless communications and radar sensing," *Proc. IEEE*, vol. 99, no. 7, pp. 1236–1259, July 2011.

[3] Y. G. Li and G. L. Stuber, *Orthogonal frequency division multiplexing for wireless communications*. Springer Science & Business Media, 2006.

[4] J. E. Palmer, H. A. Harms, S. J. Searle, and L. Davis, "DVB-T passive radar signal processing," *IEEE Trans. Signal Process.*, vol. 61, no. 8, pp. 2116–2126, April 2013.

[5] S. Mercier, D. Roque, and S. Bidon, "Study of the target self-interference in a low-complexity OFDM-based radar receiver," *IEEE Trans. Aerosp. Electron. Syst.*, pp. 1–1, 2018.

[6] F. Colone, D. W. O'Hagan, P. Lombardo, and C. J. Baker, "A multistage processing algorithm for disturbance removal and target detection in passive bistatic radar," *IEEE Trans. Aerosp. Electron. Syst.*, vol. 45, no. 2, pp. 698–722, April 2009.

[7] S. Mercier, D. Roque, and S. Bidon, "Successive self-interference cancellation in a low-complexity WCP-OFDM radar receiver," in *Proc. IEEE Asilomar Conf. Signals, Syst. Comput.*, Oct. 2018.

[8] F. Colone, R. Cardinali, and P. Lombardo, "Cancellation of clutter and multipath in passive radar using a sequential approach," in *IEEE Radar Conf.*, April 2006, pp. 7 pp.–.

[9] R. Cardinali, F. Colone, C. Ferretti, and P. Lombardo, "Comparison of clutter and multipath cancellation techniques for passive radar," in *IEEE Radar Conf.*, April 2007, pp. 469–474.

[10] Z. Zhao, X. Wan, Q. Shao, Z. Gong, and F. Cheng, "Multipath clutter rejection for digital radio mondiale-based HF passive bistatic radar with OFDM waveform," *IET Radar, Sonar Navigation*, vol. 6, no. 9, pp. 867–872, December 2012.

[11] C. Schwark and D. Cristallini, "Advanced multipath clutter cancellation in OFDM-based passive radar systems," in *IEEE Radar Conf.*, May 2016, pp. 1–4.

[12] S. Searle, D. Gustainis, B. Hennessy, and R. Young, "Cancelling strong doppler shifted returns in OFDM based passive radar," in *IEEE Radar Conf.*, April 2018, pp. 0359–0354.

[13] ——, "Aspects of delay-doppler filtering in OFDM passive radar," in *Int. Radar Conf.*, Aug 2018, pp. 1–6.

[14] D. Roque and C. Siclet, "Performances of weighted cyclic prefix OFDM with low-complexity equalization," *IEEE Commun. Lett.*, vol. 17, no. 3, pp. 439–442, March 2013.

[15] C. R. Berger, B. Demissie, J. Heckenbach, P. Willett, and S. Zhou, "Signal processing for passive radar using OFDM waveforms," *IEEE J. Sel. Top. Signal Process.*, vol. 4, no. 1, pp. 226–238, Feb 2010.

[16] L. E. Brennan and L. S. Reed, "Theory of adaptive radar," *IEEE Trans. Aerosp. Electron. Syst.*, vol. AES-9, no. 2, pp. 237–252, March 1973.

[17] E. J. Barlow, "Doppler radar," *Proc. IRE*, vol. 37, no. 4, pp. 340–355, April 1949.

[18] D. Pinchon and P. Siohan, "Closed-form expressions of optimal short PR FMT prototype filters," in *Proc. IEEE Global Telecommun. Conf.*, 2011.